HHS Public Access

Author manuscript

Osteoarthr Cartil Open. Author manuscript; available in PMC 2021 August 11.

Published in final edited form as:

Osteoarthr Cartil Open. 2021 March ; 3(1): . doi:10.1016/j.ocarto.2020.100133.

Calcium pyrophosphate crystal size and characteristics

Monica Zell, MD[a,*], **Thanda Aung, MD, MS**[b], **Marian Kaldas, MD**[b], **Ann K. Rosenthal, MD**[c], **Bijie Bai**[d,e,f], **Tairan Liu**[d,e,f], **Aydogan Ozcan, PhD**[d,e,f], **John D. FitzGerald, MD, PhD**[b]

[a]Department of Medicine, David Geffen School of Medicine, UCLA Medical Center, USA

[b]Division of Rheumatology, Department of Medicine, David Geffen School of Medicine, UCLA Medical Center, USA

[c]Division of Rheumatology, Department of Medicine, Medical College of Wisconsin, USA

[d]Department of Electrical and Computer Engineering, University of California Los Angeles, USA

[e]Department of Bioengineering, University of California Los Angeles, USA

[f]California NanoSystems Institute, University of California Los Angeles, USA

Abstract

Objective: To describe the characteristics of calcium pyrophosphate (CPP) crystal size and morphology under compensated polarized light microscopy (CPLM). Secondarily, to describe CPP crystals seen only with digital enhancement of CPLM images, confirmed with advanced imaging techniques.

Methods: Clinical lab-identified CPP-positive synovial fluid samples were collected from 16 joint aspirates. Four raters used a standardized protocol to describe crystal shape, birefringence strength and color. A crystal expert confirmed CPLM-visualized crystal identification. For crystal measurement, a high-pass linear light filter was used to enhance resolution and line discrimination of digital images. This process identified additional *enhanced* crystals not seen by raters under CPLM. Single-shot computational polarized light microscopy (SCPLM) provided further confirmation of the *enhanced* crystals' presence.

Results: Of 932 suspected crystals identified by CPLM, 569 met our inclusion criteria, and 293 (51%) were confirmed as CPP crystals. Of 175 unique confirmed crystals, 118 (67%) were rods (median area 3.6 μm^2 [range, 1.0–22.9 μm^2]), and 57 (33%) were rhomboids (median area 4.8 μm^2 [range, 0.9–16.7 μm^2]). Crystals visualized only after digital image enhancement were smaller and less birefringent than CPLM-identified crystals.

Conclusions: CPP crystals that are smaller and weakly birefringent are more difficult to identify. There is likely a population of smaller, less birefringent CPP crystals that routinely goes

*Corresponding author. UCLA Department of Medicine Ronald Reagan UCLA Medical Center, 757 Westwood Plaza, Suite 7501, Los Angeles, CA, 90095, USA. Mzell@mednet.ucla.edu (M. Zell).

Declaration of competing interest

Dr. Ozcan has a patent pending for SCPLM technology.

undetected by CPLM. Describing the characteristics of poorly visible crystals may be of use for future development of novel crystal identification methods.

Keywords

Calcium pyrophosphate; CPPD; Crystal arthropathy; Light microscopy

1. Introduction

Calcium pyrophosphate deposition (CPPD) disease is arthritis due to deposition of calcium pyrophosphate (CPP) crystals in synovial fluid or tissues, which can cause significant morbidity and is often underdiagnosed [1]. It has been regarded as a great mimicker due to its clinical heterogeneity, resembling both acute inflammatory monoarthritis and chronic polyarticular arthritis [2,3]. The presence of radiographic chondrocalcinosis is neither sensitive nor specific for clinically significant disease. The identification of CPP crystals is essential for an accurate and clinically meaningful diagnosis of CPPD disease.

Compensated polarized light microscopy (CPLM) of synovial fluid is the gold standard diagnostic method for CPP crystal-associated arthropathy [4]. However, CPP crystal size and weak birefringence makes crystal identification challenging. As a result, diagnostic accuracy is highly user-dependent [5]. Several quality control studies have underscored the poor inter-laboratory reliability of CPP identification, including false negatives, false positives and misclassification of crystals [6–9]. There is ample room for improvement in crystal identification, particularly CPP crystals, amongst rheumatologists, other clinicians, and lab technicians [10]. Lumbreras et al. demonstrated that analyst training improved the consistency of CPP crystal identification [11]. The low sensitivity of CPLM also relates to limitations of the sample and the instrument; the CPP crystal concentration threshold for detection with CPLM is higher than estimates of *in vivo* crystal concentrations [12], and CPP crystals smaller than 1 μm fall below the limit of CPLM detection [13]. Likewise, in an early report of clinical CPP arthropathy, while no crystals were detected by CPLM, abundant crystals smaller than 1 μm were identified at the ultrastructural level with electron microscopy and X-ray spectrometry [14]. Furthermore, CPP crystals are weakly birefringent, making them difficult to detect by polarized light microscopy. Ivorra et al. [15] found that fewer than 20% of CPP crystals identified under ordinary light microscopy showed birefringence under polarized light. Given the abundance of issues associated with CPP identification by CPLM, there is clear need for a more reliable diagnostic tool.

To address the inherent challenges of CPLM for crystal arthropathy diagnosis, our group developed advanced microscopic imaging methods, including a lens-free polarized imaging system that directly images crystals using a light source and complementary metal-oxide-semiconductor (CMOS) [16] and a single-shot computational polarized light microscopy (SCPLM) system that uses an industrial polarization CMOS image sensor [17]. We undertook this project to better define the size and shape of CPP crystals as a reference database for these projects. To accomplish this, we rigorously evaluated crystals, first by multi-rater assessment of slides, followed by digital photomicrograph analysis, and subsequent expert confirmation of crystals. Additionally, crystals that were not originally

seen under direct CPLM, but visualized on enhanced digital images, were confirmed using advanced microscopic imaging with SCPLM.

2. Methods

2.1. Synovial fluid and preparation of slides

A protocol to obtain de-identified CPP-positive synovial fluid samples from our institution's clinical laboratory was determined to be exempt from human subject review by our local institutional review board. Per the clinical laboratory's protocol, all samples were centrifuged for 5 min, examined, and stored at 4 °C for seven days until no longer clinically needed. Over a four-month period, CPP-positive samples were transferred to our group for storage at 4 °C. Patient information was not made available to the research team. For this study, 15 μL of fluid was aspirated from the sediment of each synovial fluid sample and smeared on a microscope slide. To enhance the durability of slides for CPLM analysis, each aspirate was air-dried and mounted with permanent mounting media and cover-slipped.

2.2. Photomicroscopy

Slides were examined using a Nikon Labophot microscope with polarizer, analyzer and attached Sony Nex-5 digital camera. Using the 100X, 0.9 NA objective, digital photographs captured an area of 55.5 μm by 83.5 μm from the area of interest on the microscopic field-of-view (FOV) diameter of 200 μm. Both the stage and analyzer were fixed and therefore crystals were randomly oriented with respect to the slow axis of polarization.

2.3. Crystal identification by multi-rater assessment and crystal inclusion criteria

Slide assessment was conducted by four independent raters; two were crystal-experienced and two were less crystal-experienced. All raters first underwent training with sample slides, which included CPP crystal-rich and crystal-free preparations. For evaluation of the study samples, raters used a standardized protocol to score each suspected crystal. Raters scanned each slide with 10x or 40x objectives using either white or polarized light until regions suspicious for CPP crystals were identified. Suspected crystals were photographed using polarized light and the 100x objective. Raters examined each slide until a minimum of 10 suspected CPP crystals were photographed, with a minimum of four FOV photographs, or until a maximum of thirty minutes was reached. Raters described suspected crystals by shape (*rod* or *rhomboid*), birefringence strength (*none, weak, moderate, strong*) and color (*blue* or *yellow-orange*), and certainty that the object was a CPP crystal (*low, medium*, or *high* certainty). Suspected crystals that raters scored as low certainty, and those with atypical shape (non-linear borders, inconsistent with rod or rhomboid shape) or uncharacteristically bright birefringence (likely artifact) as determined by the lead author were excluded from the dataset. Suspected crystals were also excluded if the quality of rater-submitted photomicrograph images limited assessment of crystal shape or precise crystal measurement.

2.4. Digital photomicrograph preparation, crystal measurement, and enhanced crystals

To facilitate accurate crystal measurement, images were digitally enhanced to improve resolution and line discrimination using a high-pass linear light filter in Adobe Photoshop CS6. CPLM-visualized crystals were measured for area, length and width (for rods), and

diagonals (for rhomboids) using the Photoshop image analysis measurement function. The acute angle of each rhomboid was calculated based on rhomboid area and diagonal lengths. Digitally enhanced images had superior clarity and contrast compared to the CPLM experience, resulting in the detection of additional low-contrast and small crystals not visible during the raters' CPLM examination. Henceforth, we refer to these newly visible crystals with digital enhancement as *enhanced* crystals, which were measured for area only.

2.5. Final crystal inclusion by expert confirmation

Finally, digital images of rater-suspected CPLM-detected crystals that met initial inclusion criteria were reviewed by a national CPP crystal expert (AR). For each of the 16 slides, only the rater assessment with the highest number of unique expert-confirmed crystals was included in the final dataset. Because *enhanced* crystals were not directly observed by raters under CPLM, they were not evaluated by the expert and therefore are not included in the primary analysis.

2.6. Single-shot computational polarized light microscopy

To more closely evaluate *enhanced* crystals detected only by digital image enhancement, but not observed under CPLM, we re-imaged select fields-of-view using our single-shot computational polarized light microscopy (SCPLM) methodology [17]. Briefly, SCPLM uses a conventional bright-field microscope (IX83, Olympus) with a standard objective lens (100x/1.4NA). A left-hand circular polarized light is used to illuminate birefringent objects, whose image is captured by a complementary metal-oxide-semiconductor (CMOS) image sensor (PHX050S-PC, LUCID Vision Labs), which has 2448 × 2048 pixels, with a pixel size of 3.45 μm. Each pixel of the CMOS image sensor is integrated with a directional polarizing filter (0°, 90°, 45°, or 135°), which enables the simultaneous detection of four different polarization components. Raw images from multiple focal depths are combined into single retardance and orientation-based views and finally combined into a single bright-field fused image.

2.7. Statistical methods

Means were compared using either student's t-test or ANOVA as appropriate. Where appropriate, comparisons of medians were analyzed using Wilcoxon two-sample test. Proportions were compared using chi-square statistics. Multivariate analysis using logistic regression examined factors associated with confirmation of crystal certainty as determined by our expert reviewer.

3. Results

3.1. Description of CPP crystal set and rater performance

Synovial fluid from 16 joint aspirates was examined. The four raters identified 932 *suspected* crystals under CPLM, from which 569 (61%) were judged as *likely* crystals (eliminating 363 *unlikely* crystals that did not meet inclusion criteria) after first pass review of digital photomicrograph images by the lead author. Subsequently, the expert reviewed digital images of *likely* crystals and determined 293 (51%) as *confirmed* CPP crystals for inclusion in the final CPLM-visualized dataset [Fig. 1]. On review of the digital images

enhanced with a high-pass filter in Adobe Photoshop, an additional 346 *enhanced* crystals meeting inclusion criteria were identified by the lead author that were not described by raters when examining under CPLM. The mean areas of *unlikely* crystals (2.2 μm^2), *rejected* crystals (4.8 μm^2), and *enhanced* crystals (2.9 μm^2) were all significantly smaller than the mean area of crystals *confirmed* by the expert (5.8 μm^2, $p < 0.05$ for all comparisons) [Fig. 2].

There was little difference in the proportion of crystals confirmed by the CPP expert between the more (51% and 55%) and less (56% and 49%) experienced raters ($p = 0.9$). Crystals that were rejected by the expert were more likely to be smaller, rhomboid, yellow-orange rather than blue, and have weaker or no birefringence. No crystals were identified by any of the four raters in 1 of 16 samples (6%) identified as CPP-positive from the clinical lab. Likewise, for 7 slides (44%), raters identified a median number of < 2 possible crystals per slide, suggesting sparse CPP crystal concentration on the slide. The remaining 8 slides (50%) had easily identified crystals.

3.2. Characteristics of CPP crystals

Of 175 unique *confirmed* CPP crystals, 118 (67%) were categorized as rods, with median area of 3.6 μm^2 (range, 1.0–22.9 μm^2), and 57 (33%) were rhomboids, with median area of 4.8 μm^2 (range, 0.9–16.7 μm^2), $p = 0.39$. Rod median length was 3.7 μm (range, 1.0–9.8 μm), median length to width ratio 3.3 (range, 1.0–13). Length correlated with length-to-width ratio ($r = 0.67$), with smaller rods more likely to have lower length-to-width ratios. Rhomboid median (maximum and minimum) diagonal lengths were 3.0 μm (range, 1.0–7.3 μm) and 2.4 μm (0.7–4.9 μm), respectively. There was little correlation between rhomboid physical size (dimensions or area) and morphology (angle). There was little variation in the ratio of the diagonals, median 1.33 (range, 1.03–1.66), or the median acute angle of rhomboids, 77.1° (range, 65.7° to 88.3°) [Table 1].

Compared to rhomboids, rods were more likely to have weak birefringence (34% vs. 12%), whereas strong birefringence was more common in rhomboids than rods (37% vs. 12%). Still, moderate birefringence was the most common classification for both rods (52%) and rhomboids (47%). The distribution of birefringence color varied from the expected 50:50, which should occur with random orientation of the crystal on the slide with fixed alignment of the axis of polarization. Of *confirmed* crystals, more blue crystals (57%) were observed than yellow-orange crystals (41%), suggesting that yellow-orange crystals were more difficult to visualize under CPLM. Only 4 (1.4%) non-birefringent *confirmed* crystals were identified [Table 1].

Enhanced crystals visualized only after the application of a digital high-pass filter were smaller and less birefringent than microscope-visible confirmed crystals. Of 346 *enhanced* crystals, 232 (67%) were rods, median area 2.4 μm^2 (range, 0.9–16.7 μm^2), 106 (31%) were rhomboids, median area 2.0 μm^2 (range, 0.5–13.8 μm^2), and 8 (2%) were too small to accurately decipher rod versus rhomboid, with a median area of 0.9 μm^2 (range, 0.4–1.6 μm^2). Overall, *enhanced* crystals had a mean area of 2.9 μm^2, half the overall mean area of *confirmed* crystals, $p < 0.001$ [Fig. 2]. In contrast to *confirmed* crystals, where a higher blue-to-yellow ratio was observed, 46% of *enhanced* crystals were yellow-orange,

while only 37% were blue. Unlike *confirmed* crystals, only 14% of *enhanced* crystals were moderately birefringent, 69% were weakly birefringent, and 16% were non-birefringent.

To further evaluate the presence of *enhanced* crystals, select slides were re-imaged with SCPLM and visually compared to the same digitally enhanced CPLM photomicrograph field-of-view [Fig. 3]. Crystals that were rejected (A and B) based on the expert's review of the digitally enhanced CPLM image (Fig. 3B) were more easily delineated on the SCPLM images (Fig. 3C and D) and likely represent crystal stacking and superimposed material, respectively, but likely still represent true CPP crystals rejected by the expert due to visualization limitations. *Enhanced* crystals are difficult to see on the untouched digital CPLM image (Fig. 3A; yellow arrows) but are clearly seen with digital enhancement (Fig. 3B), and well-visualized on the SCPLM panels (Fig. 3C and D). SCPLM also identified additional rod-like birefringent objects suggestive of CPP crystals that were not detected on the CPLM digitally enhanced image (Fig. 3C and D; orange asterisks).

4. Discussion

CPP crystal identification remains a challenge with CPLM. We sought to describe the morphologic characteristics of CPLM-detected CPP crystals. Our findings reaffirm the small size of CPLM-detected CPP crystals, with the median rod lengths and rhomboid diagonals in our dataset falling within the lowest quartile of the observed CPP crystal size range (0.4–20 μm) described in the literature [18]. Digital enhancement of CPLM images, confirmed with advanced SCPLM imaging, demonstrates that there appear to be many more, smaller and less birefringent crystals than detected by traditional CPLM. The clinical significance of this observation is unknown at this time. Future studies would need to be conducted to evaluate the clinical utility of greater crystal detection.

Our study comes with limitations. While raters' assessments were based on direct observation under CPLM, there was no feasible method whereby the expert could re-identify with CPLM the same rater-observed crystals based on slide location and morphology descriptions. Therefore, the expert's assessment was limited to examination of the raters' digital photomicrographs taken of suspected crystals observed under CPLM. There are multiple limitations of analyzing digital images rather than using microscopy for CPP crystal confirmation: viewing a single focal plane without the ability to pan across the focal depth of a crystal suspended on the slide; loss of contrast potentially obscuring crystal size and shape; and the appearance of a pinkish hue on crystals oriented perpendicular to the axis of polarization. Some of these limitations were overcome by digital enhancement with a high-pass filter, whose enhanced contrast resolution and line discrimination allowed for precise measurements of crystals. With the limitation of our single plane digital photomicrograph images, we erred conservatively to achieve the goal of high CPP certainty, and the expert was charged with favoring specificity over sensitivity, likely at the cost of excluding true CPP crystals resulting in the relatively low confirmed crystal rate of 51%. SCPLM overcomes these issues with the use of multiple simultaneous axes of polarization and images created across multiple focal planes, but was not feasible for all analyses in this study. From re-examination of rejected crystals with advanced SCPLM imaging (Fig.

3C and D; crystals A and B), we estimate that many of these are likely false negatives that would have been confirmed if the expert were able to analyze the same samples by CPLM.

In contrast to prior reports [15], we found a lower than expected proportion of non-birefringent crystals (1.4%). Our highly selective crystal confirmation process likely contributed to this phenomenon. The number of CPLM-visualized non-birefringent crystals likely was higher than that included in the final dataset, but similar to above, some may have been rejected to limit false positives, inadvertently increasing false negatives. Additionally, far more non-birefringent crystals were observed as *enhanced* crystals, suggesting the true proportion of non-birefringent crystals is higher than our final analytic set. The findings emphasize the difficulty of detecting non-birefringent crystals with CPLM. The low number of non-birefringent crystals also may be partly explained by sampling bias, where due to time constraints in their search for crystals, raters may have been more likely to seek out birefringent objects and discount non-birefringent objects as non-crystals, as demonstrated with higher rater uncertainty scores for non-birefringent crystals and higher prevalence of non-birefringent crystals in the *enhanced* crystal set.

A large number of *enhanced* crystals was noted after reviewing CPLM digital photomicrographs processed with a high-pass filter. While the expert did not evaluate these *enhanced* crystals, all passed inclusion criteria. These crystals with mostly weak birefringence had an average area half that of *confirmed* CPLM-visualized crystals, highlighting the fact that small and weakly birefringent CPP crystals often go undetected with CPLM.

The time delay to examine synovial fluid samples, with some samples stored at 4 °C for up to four months before dry-mounted slides were prepared for rater assessment does not reproduce clinical experience and renders slides acellular. However, for the sole purpose of describing crystal size, morphology, and birefringence, our methods likely did not alter these properties. While fresh synovial fluid examination within twenty-four hours is optimal [19,20], CPP crystals are known to be stable under refrigeration. McGill et al. found that although crystal counts declined, after 8 weeks CPP crystals were readily apparent in 10 of 11 samples stored at 4 °C, and neither new crystals nor changes in crystal morphology were noted [21]. An earlier report by Kerolus et al. described that abundant CPP crystals from five samples were diminished after one day and completely dissolved by 3–8 weeks [22]. However, in a response to that work, others reported CPP crystal stability after 4 weeks, to which the aforementioned authors responded that later experiments indeed resulted in similar observations in stability, as specimens with CPP crystals were observed over 9 months without complete dissolution [23]. Crystal count or concentration were not an outcome of our study. However, an inevitable limitation of using stored fluid samples is the absence of cells, often used by an examiner to judge an object’s size and to search for intracellular CPP crystals.

CPPD remains an underdiagnosed and understudied disease. We hope that greater diagnostic certainty will improve detection and subsequent management of CPPD. Advances described here and in other areas, such as dual-energy computed tomography (DECT) detection of CPP deposition [24], may help improve the understanding of this prevalent condition. Our

group has reported on lens-free polarized light microscopy and SCPLM as novel methods for crystal arthropathy diagnosis, with higher contrast and wider FOV than traditional CPLM [16,17]. Given these features, we hope these advanced imaging systems will lead to more accurate, less labor-intensive, and less operator-dependent crystal detection when compared to standard CPLM. As part of the development process, we seek to create an automated crystal detection algorithm. Our crystal dataset may identify starting parameters for a machine-learning program for CPP crystal detection based on characteristics including, size, shape, and birefringence strength.

Funding source

National Institutes of Health, Grant/Award Number: R21AR072946

References

[1]. Rosenthal AK, Ryan LM, Calcium pyrophosphate deposition disease, N. Engl. J. Med374 (2016) 2575–2584. [PubMed: 27355536]

[2]. Rosenthal AK, Ryan LM, Calcium pyrophosphate crystal deposition disease, pseudogout, and articular chondrocalcinosis, in: Koopman WJ, Moreland LW (Eds.), Arthritis & Allied Conditions, Lippincott Williams & Wilkins, Philadelphia, PA, 2005, pp. 2373–2396.

[3]. McCarty D, Crystals, joints, and consternation, Ann. Rheum. Dis42 (1983) 243–253. [PubMed: 6344808]

[4]. Zhang W, Doherty M, Bardin T, Barskova V, Guerne PA, Jansen TL, et al., European League against Rheumatism recommendations for calcium pyrophosphate deposition. Part I: terminology and diagnosis, Ann. Rheum. Dis70 (2011) 563–570. [PubMed: 21216817]

[5]. Swan A, Amer H, Dieppe P, The value of synovial fluid assays in the diagnosis of joint disease: a literature survey, Ann. Rheum. Dis61 (2002) 493–498. [PubMed: 12006320]

[6]. Schumacher HR Jr, Sieck MS, Rothfuss S, Clayburne GM, Baumgarten DF, Mochan BS, et al., Reproducibility of synovial fluid analyses. A study among four laboratories, Arthritis Rheum. 29 (1986) 770–774. [PubMed: 3718565]

[7]. Hasselbacher P, Variation in synovial fluid analysis by hospital laboratories, Arthritis Rheum. 30 (1987) 637–642. [PubMed: 3606682]

[8]. McGill NW, York HF, Reproducibility of synovial fluid examination for crystals, Aust. N. Z. J. Med21 (1991) 710–713. [PubMed: 1759919]

[9]. von Essen R, Holtta AM, Pikkarainen R, Quality control of synovial fluid crystal identification, Ann. Rheum. Dis57 (1998) 107–109. [PubMed: 9613340]

[10]. Berendsen D, Neogi T, Taylor WJ, Dalbeth N, Jansen TL, Crystal identification of synovial fluid aspiration by polarized light microscopy. An online test suggesting that our traditional rheumatologic competence needs renewed attention and training, Clin. Rheumatol36 (2017) 641–647. [PubMed: 27837341]

[11]. Lumbreras B, Pascual E, Frasquet J, Gonzalez-Salinas J, Rodriguez E, Hernandez-Aguado I, Analysis for crystals in synovial fluid: training of the analysts results in high consistency, Ann. Rheum. Dis64 (2005) 612–615. [PubMed: 15769916]

[12]. Gordon C, Swan A, Dieppe P, Detection of crystals in synovial fluids by light microscopy: sensitivity and reliability, Ann. Rheum. Dis48 (1989) 737–742. [PubMed: 2478085]

[13]. Swan A, Chapman B, Heap P, Seward H, Dieppe P, Submicroscopic crystals in osteoarthritic synovial fluids, Ann. Rheum. Dis53 (1994) 467–470. [PubMed: 7944620]

[14]. Bjelle A, Crocker P, Willoughby D, Ultra-microcrystals in pyrophosphate arthropathy. Crystal identification and case report, Acta Med. Scand207 (1980) 89–92. [PubMed: 6245562]

[15]. Ivorra J, Rosas J, Pascual E, Most calcium pyrophosphate crystals appear as non-birefringent, Ann. Rheum. Dis58 (1999) 582–584. [PubMed: 10460193]

[16]. Liu T, de Haan K, Bai B, Rivenson Y, Luo Y, Wang H, et al., Deep Learning-Based Holographic Polarization Microscopy, ACS Photonics7 (11) (2020) 3023–3034. [PubMed: 34368395]

[17]. Bai B, Wang H, Liu T, Rivenson Y, FitzGerald J, Ozcan A, Pathological crystal imaging with single-shot computational polarized light microscopy, J. Biophot13 (2020), e201960036.

[18]. Dieppe P, Swan A, Identification of crystals in synovial fluid, Ann. Rheum. Dis58 (1999) 261–263. [PubMed: 10225806]

[19]. Rosenthal AK, Mandel N, Identification of crystals in synovial fluids and joint tissues, Curr. Rheumatol. Rep3 (2001) 11–16. [PubMed: 11177766]

[20]. Pascual E, Sivera F, Andres M, Synovial fluid analysis for crystals, Curr. Opin. Rheumatol23 (2011) 161–169. [PubMed: 21285711]

[21]. McGill NW, Swan A, Dieppe PA, Survival of calcium pyrophosphate crystals in stored synovial fluids, Ann. Rheum. Dis50 (1991) 939–941. [PubMed: 1768165]

[22]. Kerolus G, Clayburne G, Schumacher HR Jr., Is it mandatory to examine synovial fluids promptly after arthrocentesis?Arthritis Rheum. 32 (1989) 271–278. [PubMed: 2930602]

[23]. McKnight KM, Agudelo C, Comment on the article by Keroluset al., Arthritis Rheum. 34 (1991) 118–120. [PubMed: 1984768]

[24]. Tanikawa H, Ogawa R, Okuma K, Harato K, Niki Y, Kobayashi S, et al., Detection of calcium pyrophosphate dihydrate crystals in knee meniscus by dual-energy computed tomography, J. Orthop. Surg. Res13 (2018) 73. [PubMed: 29622016]

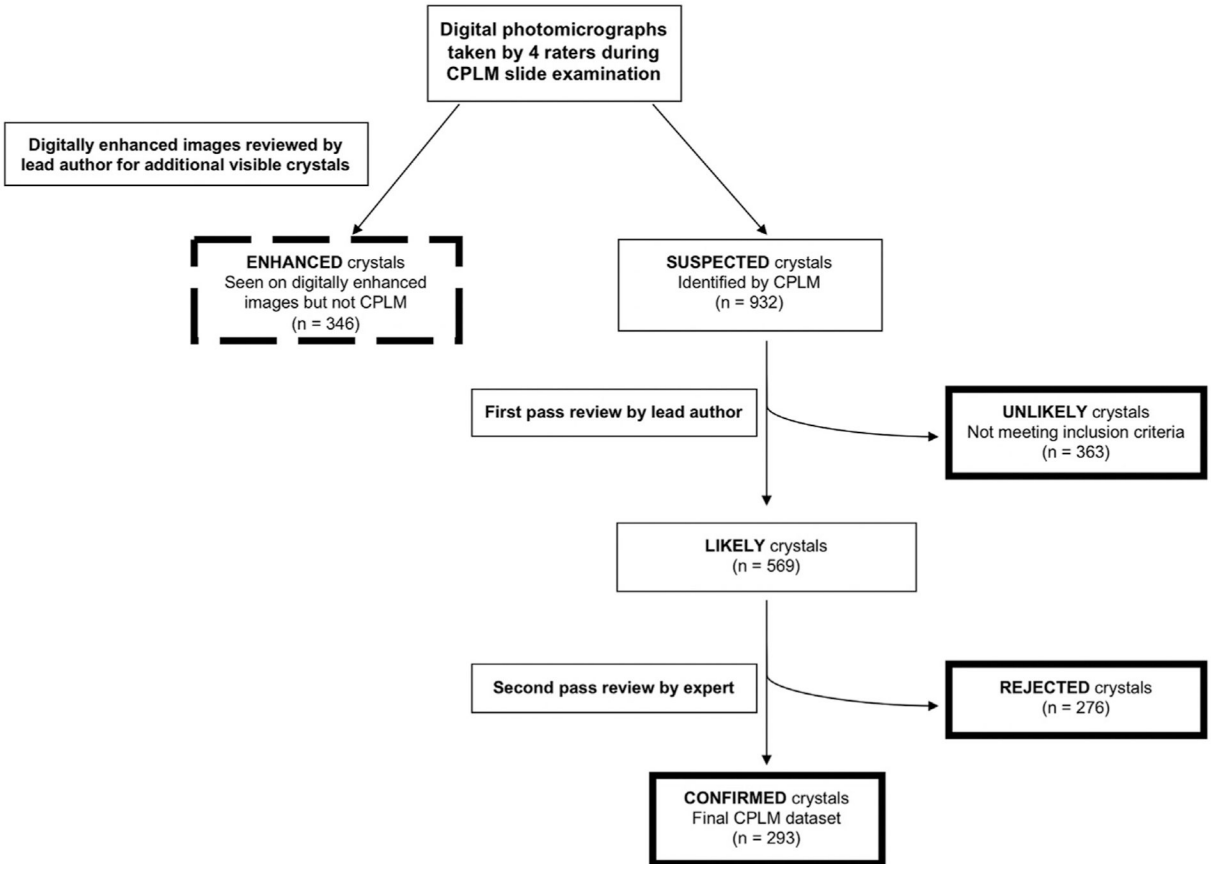

Fig. 1.

Determination of CPLM-visualized confirmed crystals and subset of enhanced crystals. 932 *suspected* crystals were identified by four raters under CPLM visualization. Upon first pass review of digital photomicrographs of the CPLM-visualized *suspected* crystals, 569 *likely* crystals met internal inclusion criteria, excluding 363 *unlikely* crystals. An expert *confirmed* 293 CPP crystals and *rejected* 276 crystals. After reviewing digital photomicrographs enhanced with a high-pass filter in Adobe Photoshop, an additional 346 *enhanced* crystals were visualized that were not detected under CPLM.

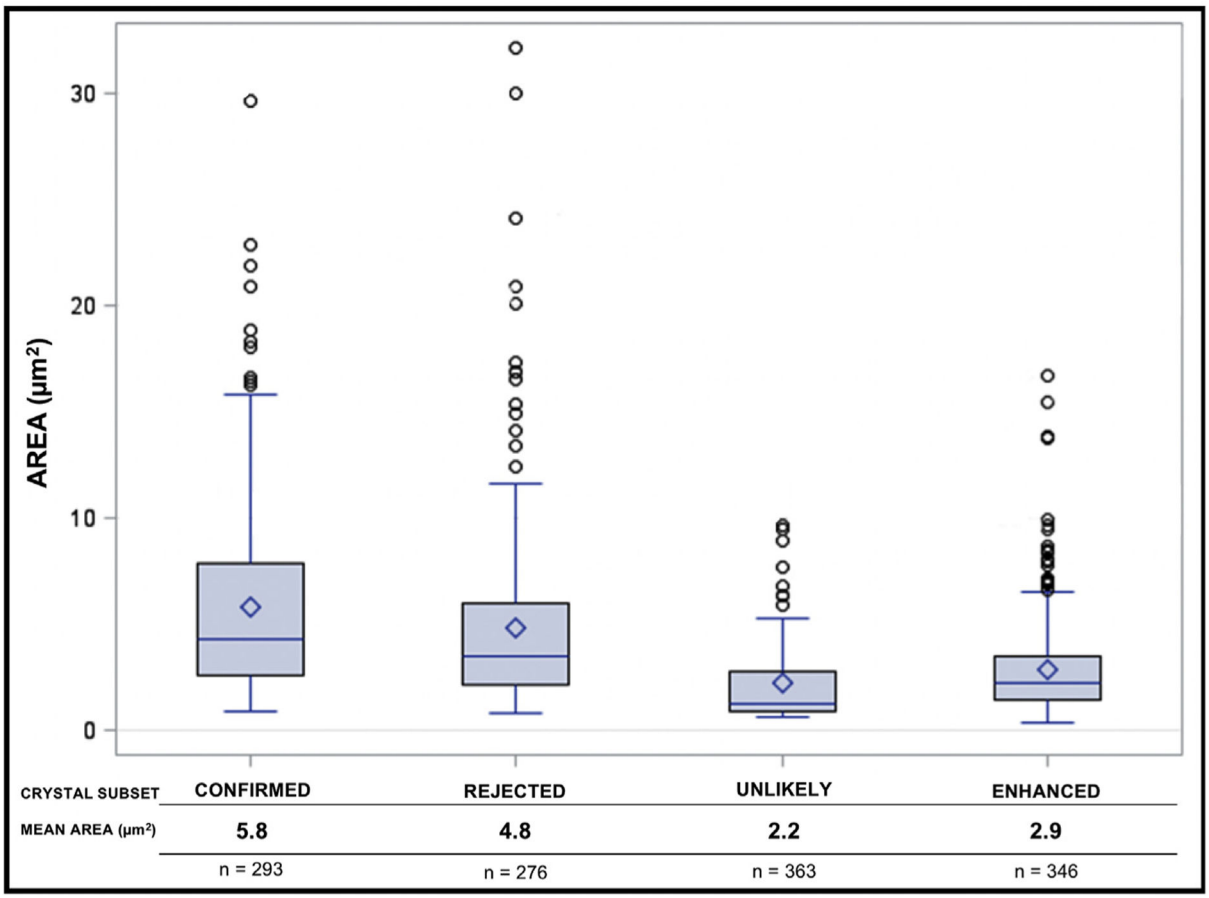

Fig. 2.

Distribution of mean CPP crystal area by crystal subset classification. Separate comparisons between all groups are significant $p < 0.001$ except for *enhanced* vs. *unlikely* crystal sizes ($p = 0.16$).

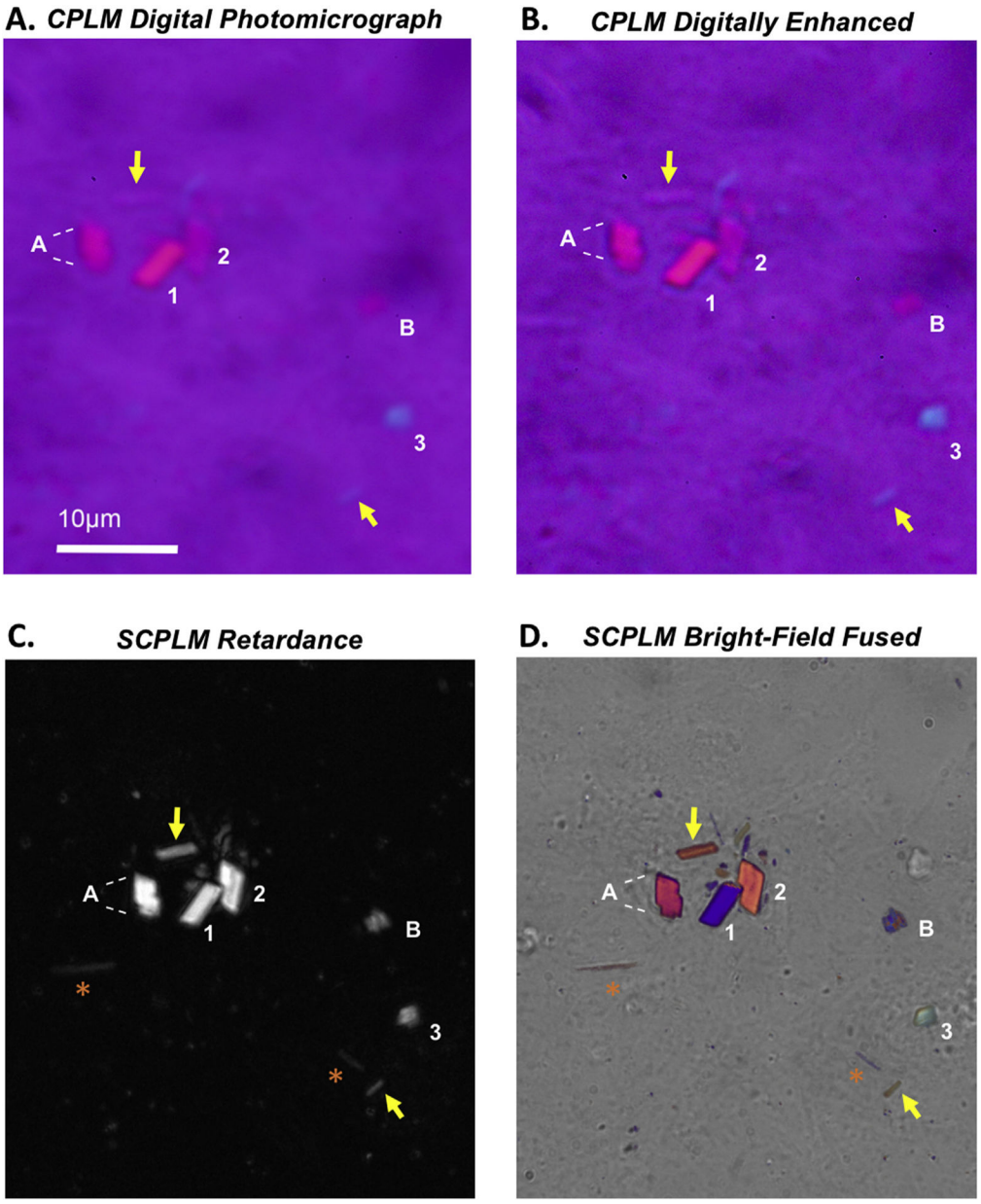

Fig. 3.

Confirmed, rejected, and enhanced crystals by CPLM and SCPLM. Select slides were re-imaged with SCPLM and visually compared to the same untouched and digitally enhanced CPLM photomicrograph 100x field-of-view. The untouched digital CPLM photomicrograph (A), which approximates the clinical CPLM experience, demonstrates the lack of contrast and line discrimination, compared to the same CPLM photomicrograph digitally enhanced with a high-pass filter in Adobe Photoshop (B). SCPLM retardance (C) and fused single bright-field (D) images demonstrate even higher levels of crystal clarity. The expert rejected crystals A and B but confirmed crystals 1–3. *Enhanced* crystals (yellow arrows) are difficult to see on the untouched digital image (A) but become clearly apparent with digital enhancement (B), and are well-visualized on the SCPLM panels (C, D). SCPLM identified

additional rod-like birefringent objects suggestive of CPP crystals that were not detected on the CPLM digitally enhanced image (orange asterisks).

Table 1

Characteristics of unique CPP crystals confirmed by expert.

	Rods (n = 118)	Rhomboids (n = 57)
SIZE (median [range])		
Area (μm^2) *	3.6 (1.0–22.9)	4.8 (0.9–16.7)
Length (μm)	3.7 (1.0–9.8)	–
Width (μm)	1.0 (0.8–1.3)	–
Length: Width	3.3 (1.0–13)	–
Diagonal max (μm)	–	3.0 (1.0–7.3)
Diagonal min (μm)	–	2.4 (0.7–4.9)
Dmax/Dmin ratio	–	1.3 (1.2–1.4)
Acute Angle (degrees)	–	77.1 (65.7–88.3)
BIREFRINGENCES (N [%])		
Strong	14 (12%)	21 (37%)
Moderate	62 (52%)	27 (47%)
Weak	40 (34%)	7 (12%)
None	2 (2%)	2 (4%)
COLOR (Among birefringent crystals, N [%])		
Blue	64 (54%)	36 (63%)
Yellow–orange	52 (44%)	19 (33%)
RATER CERTAINTY (N [%])		
High	106 (90%)	52 (91%)
Medium	10 (9%)	5 (9%)

Max = maximum; Min = minimum; D = diagonal.

* p = 0.39.